Rolling of unsaturated porous materials: Evolution of a fully saturated zone

K. Velten
Institute of Industrial Mathematics (ITWM), Erwin-Schrödinger-Straße 49, D-67663 Kaiserslautern, Germany

W. Best
Thomas Josef Heimbach GmbH & Co., Postfach 10 08 08, D-52348 Düren, Germany
(Received 16 November 1999)

When a roll moves over a partially fluid filled porous layer, the degree of saturation in the porous layer will change in an *a priori* unknown area which is affected by the roll. In this work, a mathematical model is developed that describes the saturation dynamics in the porous layer for moderate rolling velocities. The model is based on two-phase flow equations in one dimension. It can be expressed as a nonlinear second order convection-diffusion equation that can be solved by standard (upwind) finite volume techniques. The size of the area affected by the roll, and within this area the degree of saturation, fluid pressures, and fluid velocities, can be predicted. An example is studied where a fully saturated zone evolves between the rolls when the rolling velocity is increased beyond some critical value.

PACS number(s): 47.55.Mh, 81.05.Rm

I. INTRODUCTION

We consider a porous layer partially filled with a fluid which is compressed either between two rotating rolls or between a rotating roll and a fixed surface, as shown in Fig. 1. Technological applications of this process include the drying of veneers, paper, and clothes, or the extraction of wine, oil, and sugar juice (see Ref. [1]). Our starting point was an investigation of the rolling process performed by Best in Ref. [2] using paper machine press felts as a porous layer. These press felts carry the wet paper layer in paper machines, and absorb the moisture that is squeezed out from the paper during the rolling process. Based on an experimental data analysis, Best concluded (1) that a fully saturated zone evolves in press felts between the rolls under typical operational conditions, and (2) that the water is accelerated between the rolls analogously to the acceleration of water in a Venturi pipe. As we will show, the latter effect is closely related with the evolution of a fully saturated zone.

At least in the rolling of press felts and paper, the evolution of a fully saturated zone critically determines the effectiveness of the entire process, since it is obvious that press felts need to be unsaturated in some part of the rolling zone if they are to take up significant amounts of water from the paper. To clarify the basic physical principles and mechanisms that are behind the evolution of fully saturated zones in the rolling of unsaturated porous layers, a mathematical model was developed that is described in Sec. II below. The solution of the model equations is discussed in Sec. III. Referring to the rolling of a paper machine press felt as an example, it is then shown that the model predicts the evolution of a fully saturated zone in accordance with experimental observations made in the Heimbach laboratory (Sec. IV).

II. A MODEL OF THE ROLLING PROCESS

In the following, we will refer to the coordinate system and terminology introduced in Fig. 2. It is assumed that the rolls are rotating counterclockwise, and that the coordinate system is affixed at the center of the top roll, i.e., the coordinates of the center of the top roll are time independent. As a consequence, the porous layer is moving in the positive x direction. The y direction (following the roll axes) is neglected. This is a valid assumption in the case of paper machine press sections, where typical rolls are up to 10 m long, while the contact area between the felt and paper sandwich and the rolls extends only over a few centimeters (millimeters) in the x direction (z direction). The porous layer is assumed to consist of three phases, a solid phase indexed ''s'' and two fluid phases indexed ''f'' and ''g,'' which correspond to the felt fibers, the water phase, and the air phase in press sections. These three phases will be treated in the usual way as a mixture of overlapping continua, cf. Ref. [3]. Following Ref. [3], the momentum balance of the f phase can be written

$$\phi_f \rho_f \frac{D_f \mathbf{v}_f}{Dt} - \nabla \cdot \mathbf{t}_f - \phi_f \rho_f \mathbf{b}_f = \mathbf{m}_f . \tag{2.1}$$

Here, ϕ_f is the volume fraction, ρ_f (in kg/m^3) the intrinsic mass density, $\mathbf{v}_f$ (in m/s) the velocity, $\mathbf{t}_f$ (in Pa) the stress

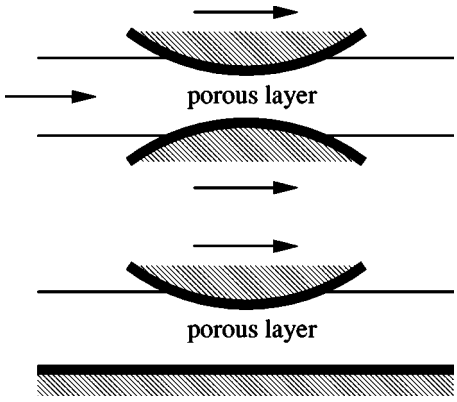

FIG. 1. A porous layer compressed between two rotating rolls (top) or between a rotating roll and a fixed surface (bottom).

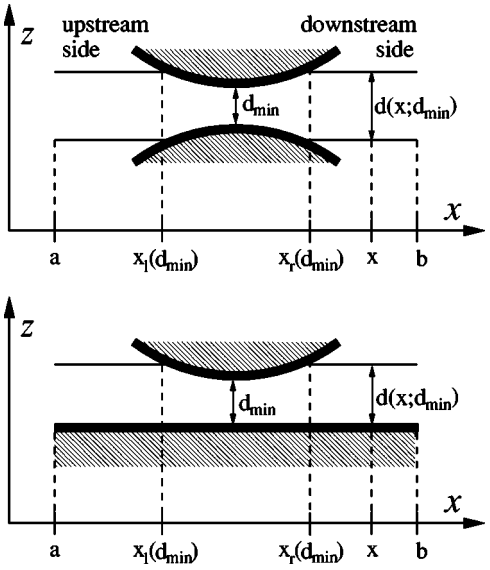

FIG. 2. Coordinate system and terminology in the case of two rotating rolls (top picture) and one rotating roll (bottom picture).

tensor, $\mathbf{b}_f$ (in N/kg) the specific body force, $\mathbf{m}_f$ (in N/m^3) the rate of momentum exchange into the f phase, and D_f/Dt signifies the material derivative in the f phase.

Considering the slow flow regime (negligible forces of inertia) under stationary conditions, treating the f phase as Newtonian, neglecting gravity, and taking the usual Stokes drag form for the momentum exchange term (see Ref. [3]), Eq. (2.1) becomes

$$\phi_f(\mathbf{v}_f-\mathbf{v}_s)=-\frac{\mathbf{K}_f}{\mu_f}\cdot\nabla p_f, \tag{2.2}$$

where μ_f (in Pa s), $\mathbf{K}_f$ (in m^2), and p_f (in Pa) are the viscosity, permeability tensor, and mechanical pressure of the f phase, and $\mathbf{v}_s$ is the velocity of the porous layer. Equation (2.2) is the two-phase flow Darcy law for the case of a moving porous medium, which means that the relative Darcy velocity $\phi_f(\mathbf{v}_f-\mathbf{v}_s)$ must be taken instead of the usual $\phi_f\mathbf{v}_f$.

The mass balance of the f phase can be written in the stationary case as [3]

$$\nabla(\phi_f\mathbf{v}_f)=0. \tag{2.3}$$

The g phase is neglected, and assumed to be essentially at atmospheric pressure, i.e., $p_g\equiv 0$, which is the well known Richards assumption. As emphasized in Ref. [4], this assumption does not imply that the g phase is stagnant, but rather the opposite: it has a very high mobility (small pressure gradients suffice to initiate g-phase flow). In our case, the Richards assumption is justified by our emphasis on the slow flow regime.

We are interested in the flow regime between x coordinates a and b in Fig. 2, where it is assumed that for $x\notin[a,b]$ the three phases are essentially at rest (in a frame of reference affixed to the solid phase). Although the real flow pattern between a and b is undoubtedly two-dimensional, a number of models have been investigated in the case of wet pressing which assume one-dimensional flow either in the x direction [5–7] or in the z direction [8–12]. Based on these models, considerable improvements in the understanding of this process have been achieved. An example is the general shape of the water pressure function $p(x)$, which was predicted in Ref. [6] and then experimentally verified by Beck in Ref. [13]. In particular, Beck found the pressure peak to be located *before* the center of the rolling zone, as predicted in Ref. [6] and also by Wahlström in Ref. [14], based on theoretical arguments.

Whether it is reasonable to consider an x-direction flow model or a z-direction flow model depends on the aspects of the rolling process which one wants to understand. If one asks what determines the evolution of a fully saturated zone in a rolling process, one will certainly find the f-phase flow in the x direction, v_f^x, among the most important factors, since it determines the rate at which the f phase is transported into the rolling zone. We have therefore decided to investigate an x-direction flow model, neglecting the z dimension. Then, referring to Eqs. (2.2) and (2.3), the momentum and mass balances become

$$\phi_f(v_f-v_s)=-\frac{K_f}{\mu_f}p_f', \tag{2.4}$$

$$(d\phi_f v_f)'=0, \tag{2.5}$$

where the tensor and vector quantities are now numbers referring to the x direction, and the prime signifies the x derivative. In the following, it will be assumed that the solid velocity v_s in Eq. (2.4) is a constant reflecting the velocity of the roll surfaces in the x direction. This means that small differences in the x-direction velocity implied by the circular geometry of the roll surfaces are neglected, an assumption which can be safely made in the case of paper machine press sections where typical roll diameters are above 1000 mm, while the indentation of the felt is about one millimeter.

A new function $d(x;d_{min})$ has been introduced in Eq. (2.5) which expresses the thickness of the porous layer as a function of x and the minimum distance between the roll surfaces, d_{min} (see Fig. 2). We will refer to d as the ''shape function.'' Note that the mass balance equation (2.5) implies a ''no flow''-condition on the top and bottom surfaces of the porous layer, i.e., the f phase is not allowed to escape through these surfaces. This is in partial contradiction with the reality in the case of press felts, since it is observed that water can escape through the top and bottom surfaces of a felt close to the center of the rolling zone, particularly at the downstream side. We will come back to this point later. Let us just remark here that it is easy to account for any available quantitative information on water losses near the rolling zone just by adding an appropriate source term at the right hand side of Eq. (2.5).

Besides v_f^x, the shape function d is another key factor determining the evolution of the fully saturated zone. While v_f^x determines the rate at which the f phase is transported into the rolling area, d determines the space available for f-phase storage. We assume that—as it is the case in paper machine press sections—the shape function d is determined from the equilibrium of forces

$$F_f+F_s=F, \tag{2.6}$$

where F_f and F_s denote the line forces exerted by the f phase, and the solid phase on the rolls, while F is the line force exerted by the rolls on the f phase and on the solid phase. These forces have units (N/m) which are to be understood as ''force per m length of the rolls in the y direction.'' We remark that Eq. (2.6) expresses the classical Terzaghi principle as discussed in Ref. [8]. To connect Eq. (2.6) with our previous equations, it is necessary to have a model for the deformation of the porous layer. Since paper machine press felts behave viscoelastically (see Ref. [15]), we choose a viscoelastic model. Precisely, we assume that the felt deforms in the z direction only following a nonlinear Kelvin-Voigt law

$$\tau_{zz}(t)=E(\epsilon(t))+\Lambda\frac{d}{dt}E(\epsilon(t)), \tag{2.7}$$

which may be written as

$$\tau_{zz}(x)=E(\epsilon(x))+v_s\Lambda\frac{d}{dx}E(\epsilon(x)), \tag{2.8}$$

using the transformation $x=v_st$. We will now describe how $d(x;d_{min})$ is determined for a given d_{min}. For $x<x_l(d_{min})$ (Fig. 2), $d(x;d_{min})=d_0$, where d_0 is the uncompressed thickness of the porous layer. For $x\in[x_l(d_{min}),x_r(d_{min})]$, $d(x;d_{min})$ follows the geometry of the roll surfaces until τ_{zz} becomes zero at $x=x_r(d_{min})$. For $x>x_r(d_{min})$, $\tau_{zz}=0$, and hence according to Eq. (2.8) the strain $\epsilon(x;d_{min})$ can be determined from the ordinary differential equation

$$\frac{d}{dx}E(\epsilon)=-\frac{1}{v_s\Lambda}E(\epsilon), \tag{2.9}$$

using the given inital value $E[\epsilon(x_r(d_{min});d_{min})]$. Then by definition of the strain, one obtains

$$d(x;d_{min})=d_0[1+\epsilon(x;d_{min})]. \tag{2.10}$$

F_f and F_s in Eq. (2.6) can now be written as

$$F_f(d_{min})=\int_{x_l(d_{min})}^{x_r(d_{min})}p_f\,dx, \tag{2.11}$$

$$F_s(d_{min})=\int_{x_l(d_{min})}^{x_r(d_{min})}\left(E(\epsilon(x;d_{min}))+v_s\Lambda\frac{d}{dx}E(\epsilon(x;d_{min}))\right)dx. \tag{2.12}$$

Note that in Eq. (2.12) ϵ is obtained from d via Eq. (2.10). Equations (2.11) and (2.12) transform Eq. (2.6) into

$$\int_{x_l(d_{min})}^{x_r(d_{min})}\left(p_f+E(\epsilon(x;d_{min}))+v_s\Lambda\frac{d}{dx}E(\epsilon(x;d_{min}))\right)dx=F. \tag{2.13}$$

Now our model consists of Eqs. (2.4), (2.5), and (2.13) for the unknowns $p_f(x)$, $v_f(x)$, $\phi_f(x)$, and d_{min}. Obviously, an additional constitutive relation is needed to close the system. As explained in Ref. [3], it is appropriate here to use the relation between capillary pressure p_c and saturation S which can be measured. The capillary pressure is defined as $p_c=p_g-p_f$ which means $p_c=-p_f$ in our case, since we assume $p_g=0$; the saturation is $S=\phi_f/\phi$, where ϕ is the porosity (ratio between void and total volume). Now, if $S=g(p_f)$ expresses the known relation between saturation and f-phase pressure, then Eqs. (2.4) and (2.5) can be written as

$$\phi g(p_f)(v_f-v_s)=-\frac{K_f(\phi,g(p_f))}{\mu_f}p_f', \tag{2.14}$$

$$(d\phi\, g(p_f)v_f)'=0. \tag{2.15}$$

Assuming that the compression of the solid phase is negligible compared with the compression of the open pore spaces, the porosity $\phi(x;d_{min})$ can be computed from $d(x;d_{min})$, using

$$d_0\phi_0-d(x;d_{min})\phi(x;d_{min})=d_0-d(x;d_{min}). \tag{2.16}$$

The latter equation says that ''the difference between the uncompressed open pore volume and the open pore volume at some coordinate x equals the total reduction of volume.''

We have parametrized the function $g(p_f)$ as

$$g(p_f)=\begin{cases}\dfrac{1}{\dfrac{1}{1-s_\infty}+\left(\dfrac{p_f}{a}\right)^n}+s_\infty, & p_f\leqslant 0\\ 1, & p_f>0,\end{cases} \tag{2.17}$$

where $0<s_\infty<1$, $a<0$, $n>1$ (see Ref. [16] for various other parametrizations). For our following discussion, it is important to note (a) that saturation values $S=g(p_f)<1$ correspond to negative p_f values, and (b) that $g(p_f)$ is a bijection for saturation values $S<1$. As it is indicated in Eq. (2.14), we assume another constitutive relation for K_f which is expressed as a nonlinear function of porosity and saturation as

$$K_f(\phi,S)=k\frac{\phi^3}{1-\phi^2}S^m, \tag{2.18}$$

where $k>0$ and $m>1$. Similar expressions for K_f were used, e.g., in Refs. [17] and [9]. The factor $\phi^3/(1-\phi^2)$ originates from the Kozeny-Carman equation (see Ref. [18]), which is a widely used empirical expression relating porosity and permeability. The factor S^m is needed since $K_f(S,\phi)$ is a *relative* permeability; see the discussion in Refs. [3] and [17]. This factor reduces K_f if the saturation decreases, since in that case the network of flow channels which is available for f-phase flow becomes smaller. Finally, boundary conditions must be defined. It is natural to require

$$\lim_{x\to-\infty}S(x)=S_0 \tag{2.19}$$

and

$$\lim_{x\to\infty}v_f(x)=v_s. \tag{2.20}$$

Equation (2.19) means that the saturation in the upstream direction ''far away from the rolling area'' is known. Equa-

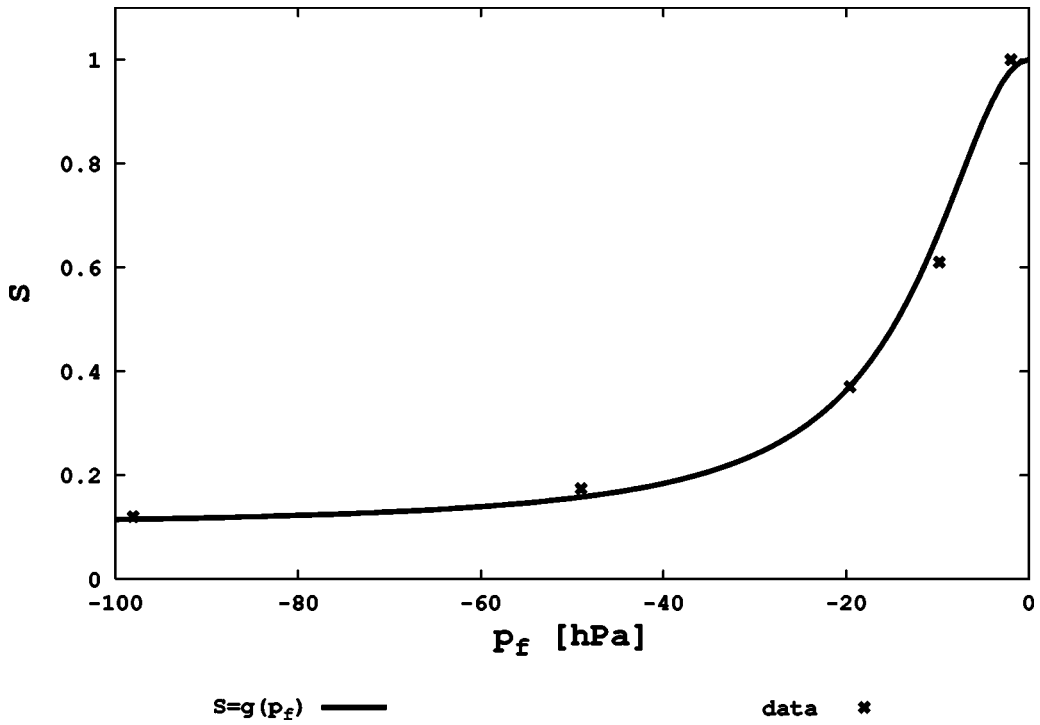

FIG. 3. Saturation-pressure function $g(p_f)$.

tion (2.20) means that ''far away from the rolling area'' in the downstream direction there is no *f*-phase flow relative to the movement of the porous layer. We will restrict our attention to the case $S_0<1$ in the following, since we are interested in the evolution of a fully saturated zone from unsaturated conditions.

III. SOLUTION OF THE MODEL EQUATIONS

For some given $d_{min}>0$, Eqs. (2.14) and (2.15) can be expressed as

$$-\left(\frac{K_f[\phi(x;d_{min}),g(p_f(x))]}{\mu_f}p_f'(x)\right)' + [d(x;d_{min})\phi(x;d_{min})g(p_f(x))v_s]'=0, \tag{3.1}$$

which is a nonlinear convection-diffusion equation (cf. Ref. [19]) in the unknown $p_f(x)$. The boundary conditions (2.19) and (2.20) can be approximated by

$$p_f(-C)=p_0:=g^{-1}(S_0), \tag{3.2}$$

$$p_f'(C)=0 \tag{3.3}$$

for some large $C\in R_+$ [use Eq. (2.4) together with Eq. (2.20) to obtain Eq. (3.3)]. After linearization, the system (3.1)–(3.3) can be solved by some standard finite volume discretisation [20]. Upwinding must be used for high values of the convective velocity, i.e., for high porous layer velocities v_s [19]. *C* must be chosen large enough such that no influence of *C* on the solution p_f can be observed.

If Eqs. (3.1)–(3.3) is solved for some given d_{min}, the resulting $p_f(x;d_{min})$ can be inserted into Eq. (2.13). Then Eq. (2.13) is a nonlinear equation in the remaining unknown d_{min} which can be solved, e.g., by bisection until the equilibrium d_{min}^* is found.

IV. EXAMPLE

As an example we take the rolling of a wet press felt as it is used in paper machines. We assume that the press felt is rolled as it is, i.e., without a paper layer. The following parameter values represent a typical situation in a press section of a paper machine (most of the measurement values are from the laboratories of Heimbach and JWI[1]): The water viscosity μ_f was set to 4.7×10^{-4} Pa s, which corresponds to a temperature of 60 °C. In the expression for the relative permeability K_f [Eq. (2.18)], the permability factor *k* was set to $k=10^{-10}$ m^2, and the exponent *m* was set to 3.4 following Ref. [9]. For the saturation-pressure function $g(p_f)$ we took the data shown in Fig. 3 which were fitted to Eq. (2.17). For the stress-strain function $E(\epsilon)$ we took the data shown in Fig. 4, which were fitted to

$$E(\epsilon)=\epsilon^r. \tag{4.1}$$

The viscoelastic time constant Λ was set to 0.4 ms (this is in the same order of magnitude as Λ values that may be derived from measurements of ''felt-springback'' given in Ref. [15]). If not stated otherwise below, the remaining data are $d_0=2.5$ mm, $\phi_0=0.52$, and $S_0=0.5$; the radius of the rolls is $R=100$ mm, and $F=70$ kN/m.

Simulation results for rolling velocities between $v_s=0.0001$ and 50 m/min will be discussed. We restrict our attention to this range of velocities since it can be shown that

[1]JWI Ltd., 48 Richardson Rd., Kanata, Ont. L2L 1X2.

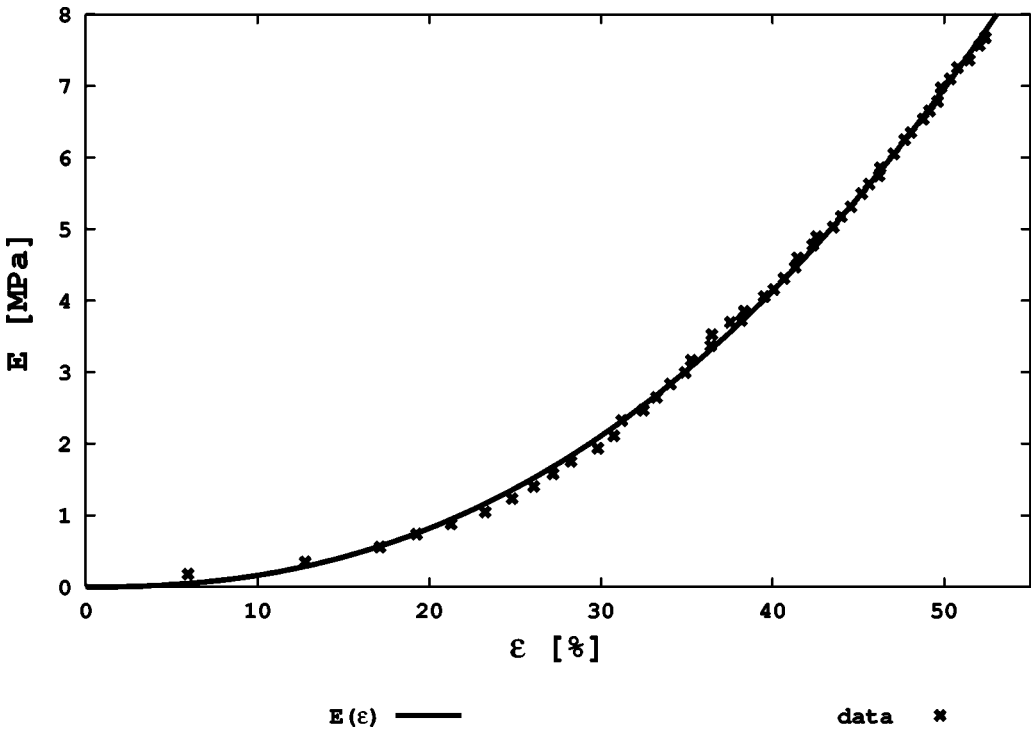

FIG. 4. Stress-strain function $E(\epsilon)$.

beyond $v_s = 50$ m/min inertial forces become important (i.e., the first term on the left hand side of Eq. (2.1) reaches the same order of magnitude as the stress and momentum exchange terms). The saturation profiles are shown in Figs. 5 and 6, and corresponding pressure profiles in Figs. 7 and 8.

The area of contact between the felt and the rolls was approximately between -21.3 and $+21.3$ mm for small rolling velocities, and between -20.9 and 20.1 mm for $v_s = 50$ m/min. This decrease of the contact area was both due to the fact that the roll distance d_{min} increased with the machine velocity (see below), and it was due to the viscoelastic effect which caused a stronger reduction of the contact area at the downstream side (by 1.2 mm) compared to the upstream side (0.4 mm). As Figs. 5 and 7 show, $v_s = 0.0001$ m/min practically corresponds to the standing machine, i.e., the water pressure between the rolls remains unchanged and the satu-

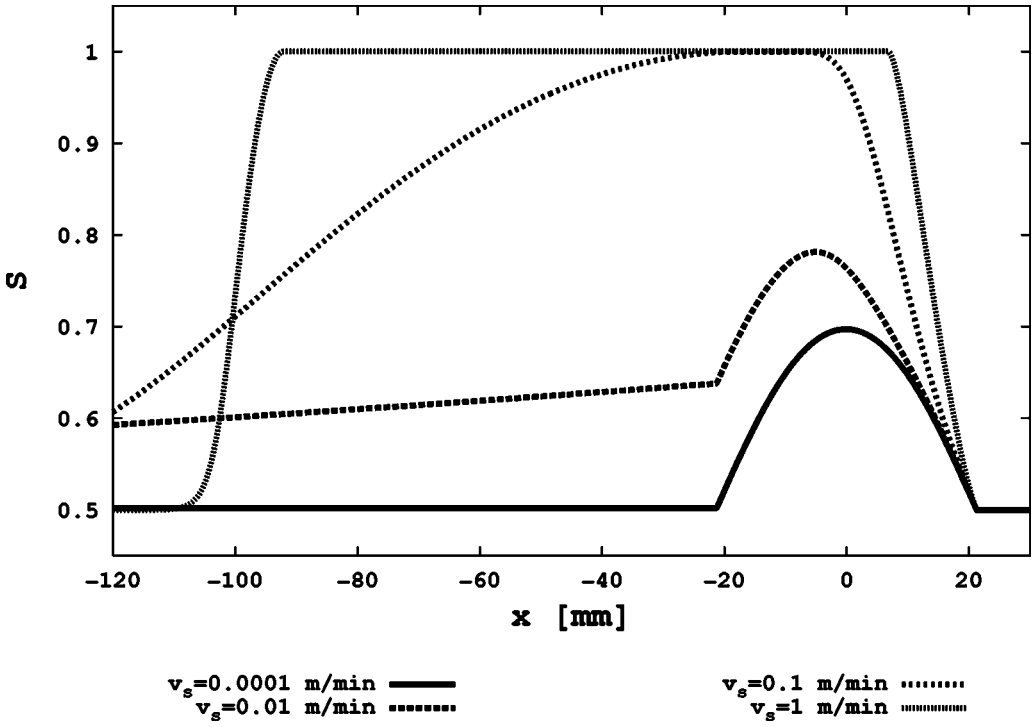

FIG. 5. Saturation profiles for solid velocities between $v_s = 0.0001$ and 1 m/min.

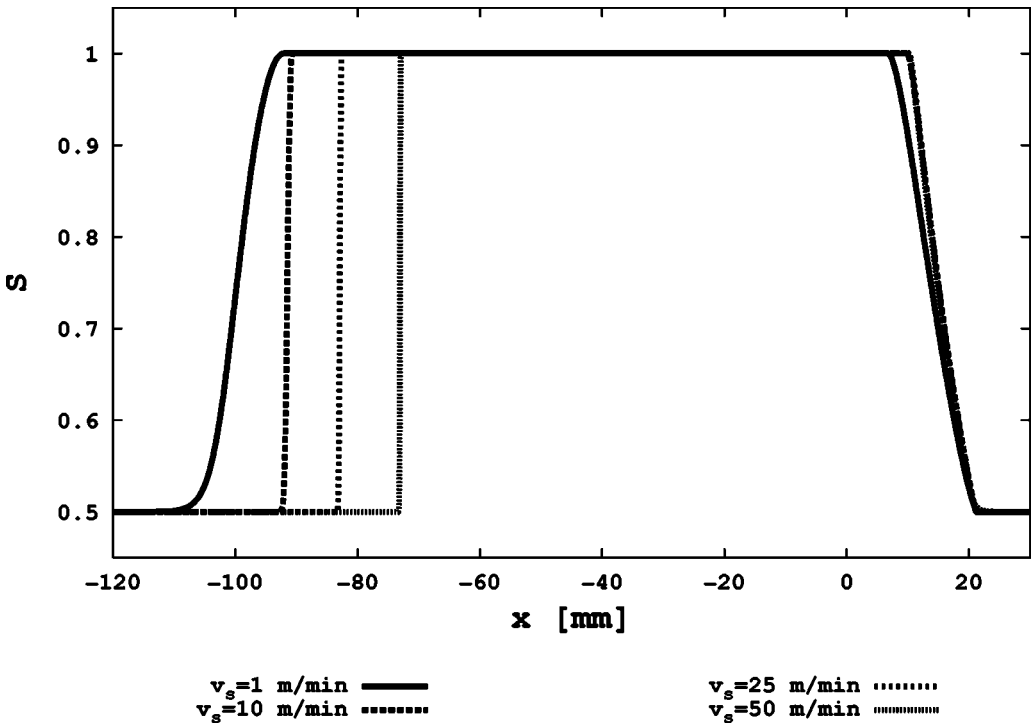

FIG. 6. Saturation profiles for solid velocities between $v_s = 1$ and 50 m/min.

ration profile shows a symmetric increase around the center of the rolling zone at $x = 0$ mm, reflecting the decrease of the porosity ϕ in the rolling zone.

At $v_s = 0.01$ m/min, the saturation profile becomes unsymmetric since an increase of the saturation at the upstream side superimposes the symmetric ''standing machine'' saturation profile. As Fig. 7 shows, there is a corresponding pressure rise at the upstream side of the rolling zone. At $v_s = 0.1$ m/min, the water pressure is more than atmospheric ($p_f > 0$) in a small area upstream of the rolling zone center $x = 0$, which corresponds to full saturation $S = 1$ as explained above. At $v_s = 1$ m/min, the porous layer is fully saturated about 70 mm before the first contact between felt and rolls at about -20 mm, and the water pressure peak is now markedly above zero (about 8000 Pa). As the velocity v_s is further increased, the fully saturated area at the upstream side becomes smaller again, while the pressure peak increases continuously up to a level of about 0.3 MPa at $v_s = 50$ m/min

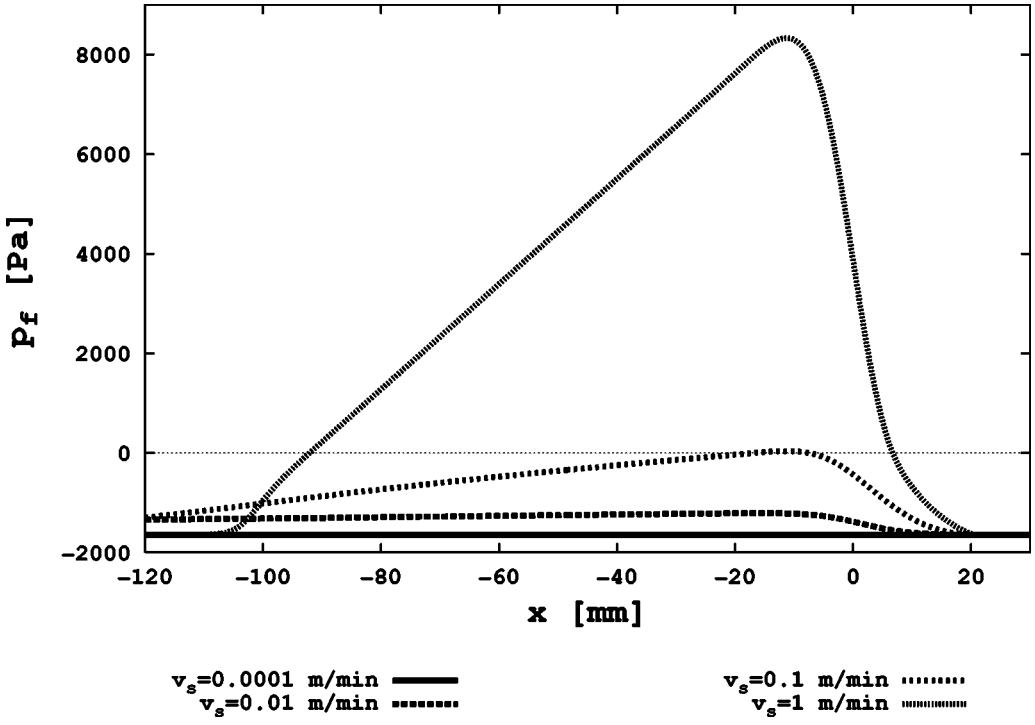

FIG. 7. Pressure profiles for solid velocities between $v_s = 0.0001$ and 1 m/min.

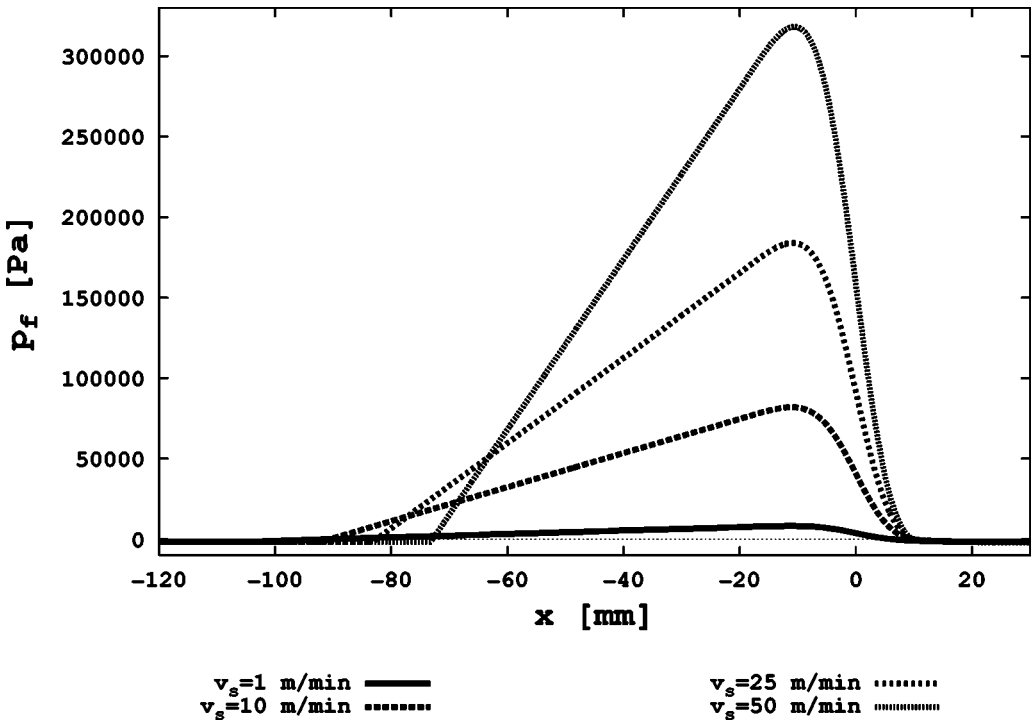

FIG. 8. Pressure profiles for solid velocities between $v_s=1$ and 50 m/min.

(Figs. 6 and 8).

Figures 9 and 10 show the development of $(v_f-v_s)/v_s$ depending on the machine velocity v_s. We refer to $(v_f-v_s)/v_s$ as the ''specific relative fluid velocity,'' since it measures the movement of the water relative to the felt in v_s units. As the figures show, the relative movement of the water in the felt is always opposite to the machine direction at the upstream side of the roll and in the first part of the rolling area. Close to the center of the rolling zone, however, the water is accelerated until a maximum velocity is reached at $x=0$. At maximum velocity, the water is more than 40% faster than the felt for all felt velocities $v_s \leqslant 50$ m/min.

Figure 11 shows the development of the line forces exerted by the felt and the water phase on the rolls, F_s and F_f. As it can be seen, F_f begins to increase at about $v_s=1$ m/min, until it becomes $F_f=6.5$ kN/m or 10.2% of F_s

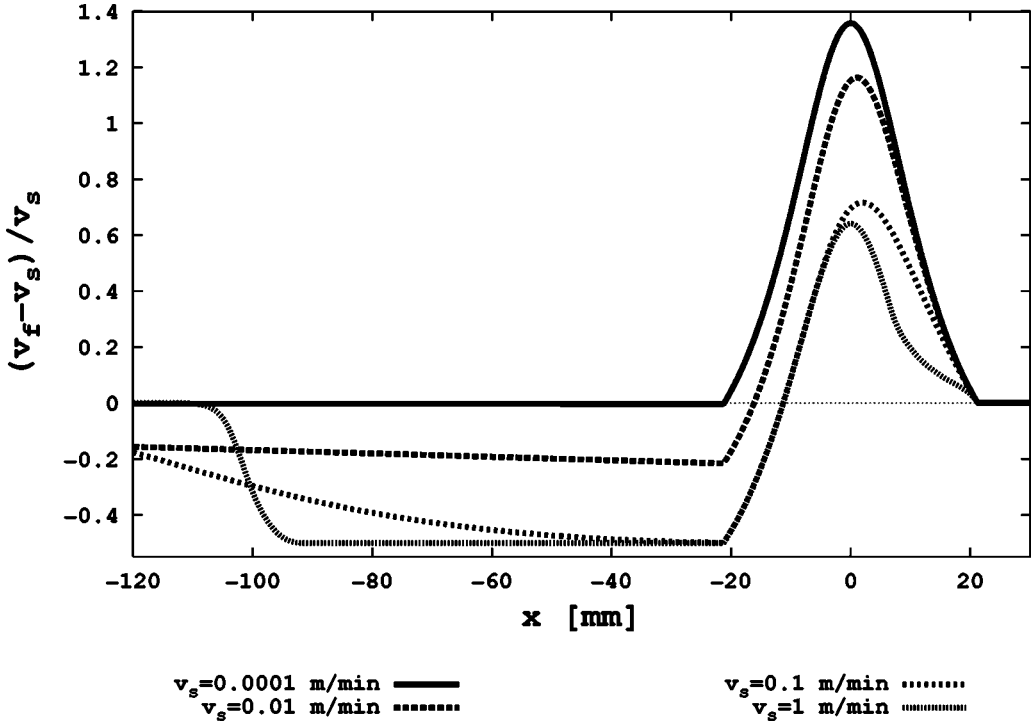

FIG. 9. Specific relative fluid velocity profiles for solid velocities between $v_s=0.0001$ and 1 m/min.

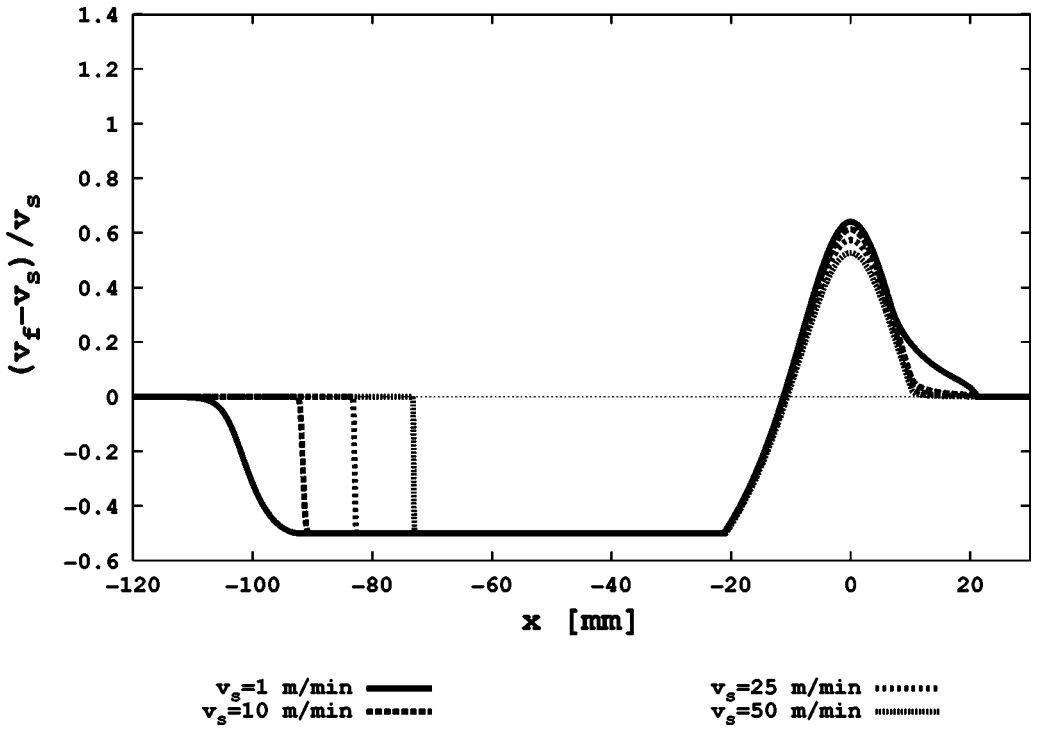

FIG. 10. Specific relative fluid velocity profiles for solid velocities between $v_s = 1$ and 50 m/min.

$=63.5$ kN/m at $v_s = 50$ m/min. The sum of F_f and F_s always equals the line force exerted by the rolls on the water-felt system, $F = 70$ kN/m, as required by Eq. (2.6). The figure also shows the equlibrium distance between the rolls, d_{min}. As a consequence of the increasing F_f, d_{min} also increases, i.e., the pressure in the water phase forces the rolls to increase their distance.

The simulation results reflect important qualitative characteristics of the rolling process in paper machines. As mentioned in Sec. I, the acceleration of the water phase in the rolling zone has already been postulated in Ref. [2] based on an experimental data analysis. The increase of d_{min} was verified on an experimental paper machine in the Heimbach laboratory. The pressure profiles in the above simulations reflect the qualitative pattern of measured pressure profiles in Ref. [13]. In particular, the pressure peak is located before the center of the rolling zone, as reported by Beck in Ref. [13].

Beck measured pressure peaks between 70 000 Pa and 1.2 MPa depending on the initial saturation of the felt. Unfortunately, a comparison with our results is difficult since Beck's results refer to a machine velocity of 381 m/min, which is in

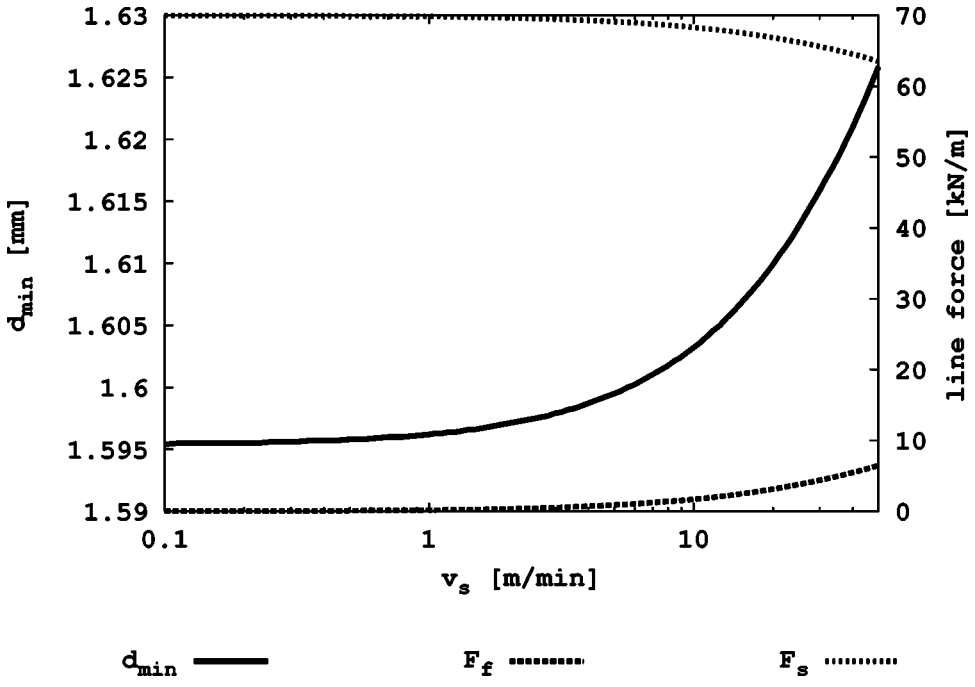

FIG. 11. Line forces and d_{min}.

the high velocity regime where inertial forces are important. Also, Beck used a much smaller roll diameter (15.54 cm instead of 100 cm in our case) and there is no or no clearly interpretable information on key parameters such as the felt permeability or the initial felt saturation. At least, it seems that the pressure peak of 300 000 Pa computed by our model for a machine velocity of 50 m/min is in the right order of magnitude.

The upstream side fully saturated zone that develops in the simulations can be associated with a water wedge that is observed at the upstream side of the rolls in paper machines [6]. According to observations made at an experimental paper machine in the Heimbach laboratory, this water wedge becomes smaller for machine velocities above $v_s = 1$ m/min, which parallels the above simulation results. At about $v_s = 500$ m/min, the water wedge disappears, and some water is seen to spray off at the downstream side of the rolls. We thus conjecture that simulations beyond $v_s = 50$ m/min will show that the fully saturated zone will be further reduced on the upstream side until it is covered by the rolls again. The fact that water sprays off at the downstream side is probably due to the combined effect of the downstream-moving fully saturated zone on the one hand, and the upstream-moving downstream end of the felt-rolls contact area (caused by the viscoelastic effect) on the other hand. We are currently implementing inertial forces into our model for a further investigation of this effect.

Regarding the boundary conditions at the top and bottom surfaces of the felt, it was said above in our discussion of Eq. (2.5) that we are currently assuming ''no flow'' conditions. Of course, the upstream side water wedge as well as the fact that water sprays off at the downstream side at higher velocities show that this condition is partially violated in reality. The latter effect can be safely neglected, since we focus on the slow flow regime here, referring to velocities up to $v_s = 50$ m/min, where there are only negligible water losses observed at the downstream side of the rolls. The upstream side water wedge, on the other hand, undoubtedly violates the ''no flow'' condition, since at that point water crosses the top and bottom surfaces of the felt. However, it is important to note that this does not mean any net losses since the water wedge is stationary if v_s is kept fixed. Then, any water volume that flows from the felt into the wedge is replaced by an equivalent volume flowing backwards into the felt, forced by the downstream moving surfaces of the rolls. Thus at the upstream side our use of a no flow condition can be seen as an approximation of the real situation where there is ''no net flow'' through the felt surfaces.

V. CONCLUSIONS

A model has been developed that can be used to analyze the evolution of a fully saturated zone in processes involving the rolling of unsaturated porous materials. The model has been expressed as a nonlinear convection-diffusion equation that can be solved by (upwind) finite volume techniques. It was shown that the model correctly reproduces qualitative characteristics of paper machine rolling processes. Although the model was developed with a focus on paper machine rolling processes, we expect that it will be useful for an analysis of other rolling processes too. In current models of sugar cane rolling, for example, the location and size of the fully saturated zone is not computed but *assumed a priori* [21]. We are currently developing extensions of the existing models for sugar cane pressing based on a replacement of the viscoelastic part of our model by a model that includes the plastic deformation of sugar cane. Also, we are extending our model to account for multiple dimensions and the high velocity regime.

[1] W. Pankoke, *Continuous Press Technology* (Verlag Moderne Industrie, Landsberg/Lech, 1997).
[2] W. Best, Das Papier **41**, 55 (1987).
[3] M. Allen, G. Behie, and J. Trangenstein, *Multiphase Flow in Porous Media* (Springer, Berlin, 1988).
[4] R. Ewing, R. Lazarov, J. Pasciak, and A. Vassilev (unpublished).
[5] C. Asklöf, K. Larsson, J. Linderoth, and P. Wahlström, Pulp Pap. Mag. Can. **65(6)**, T246 (1965).
[6] J. Wilder, Tappi J. **50**, 180 (1967).
[7] S. M. C. S. Yih, Tappi J. **47**, 153 (1967).
[8] K. Hiltunen (unpublished).
[9] K. Jewett, W. Ceckler, L. Busker, and A. Co, in *New Process Alternatives in the Forest Products Industry*, AIChE Symposium Series Vol. 76 (AIChE, New York, 1980), pp. 59–70.
[10] K. Jönsson and B. Jönsson, AIChE J. **38**, 1340 (1992).
[11] K. Jönsson and B. Jönsson, AIChE J. **38**, 1349 (1992).
[12] H. Westra, Pap. Technol. Ind. **16**, 165 (1975).
[13] D. Beck, in *TAPPI Engineering Conference Proceedings* (TAPPI, Atlanta, GA, 1983), pp. 475–487.
[14] P. Wahlström, Pulp Pap. Mag. Can. **61**, T379 (1960).
[15] Z. Szikla, Pap. Timber **73**, 160 (1991).
[16] J. Bear, *Introduction to Modeling of Transport Phenomena in Porous Media* (Kluwer, Dordrecht, 1990).
[17] K. Hiltunen, J. Phys. D **25**, 1053 (1992).
[18] J. Bear and A. Verruijt, *Modeling Groundwater Flow and Pollution* (Reidel, Dordrecht, 1987).
[19] H. Roos, M. Stynes, and L. Tobiska, *Numerical Methods for Singularly Perturbed Differential Equations* (Springer, Berlin, 1996).
[20] H. Versteeg and W. Malalasekera, *An Introduction to Computational Fluid Dynamics: The Finite Volume Method* (Longman Scientific & Technical, New York, 1995).
[21] D. Owen, S. Zhal, and J. Loughran, Eng. Comput. **12**, 281 (1995).